JOURNAL OF GEOPHYSICAL RESEARCH, VOL. 112, D12208, doi:10.1029/2006JD007686, 2007

On the use of nonmethane hydrocarbons for the determination of age spectra in the lower stratosphere

D. H. Ehhalt,[1] F. Rohrer,[1] D. R. Blake,[2] D. E. Kinnison,[3] and P. Konopka[4]

Received 22 June 2006; revised 2 February 2007; accepted 14 March 2007; published 23 June 2007.

[1] On 9 April 2001, while approaching the West Coast of the North American continent, flight 20 of the NASA TRACE P campaign penetrated deeply into a stratospheric intrusion. From measurements aboard that flight we derive vertical profiles of nonmethane hydrocarbons (NMHCs) and other short-lived trace gases in the lower stratosphere using Dichlorofluoromethane, CF_2Cl_2, as the altitude scale. All profiles show an exponential decrease, which permits the description of their vertical distribution by a single parameter, the scale height. These scale heights are shown to be related to the respective lifetimes in a unique fashion. Using the approximation of a 1-D diffusive model with a constant eddy diffusion coefficient, K, and assuming constant lifetimes, we establish an analytical solution for this relation. By fitting this theoretical expression to the experimental data we can estimate K and thus obtain an approximate age spectrum of the form given by Hall and Plumb (1994). A much better fit to the experimental scale heights is obtained, when we allow the lifetimes to be height-dependent and calculate the theoretical scale heights numerically from a 1-D model. An optimization also suggests a constant K, but with a value of 0.46 m^2/s, larger than those obtained from the fit of the analytical solution. The obtained age spectra should be valid for transit times not longer than 300 days.

Citation: Ehhalt, D. H., F. Rohrer, D. R. Blake, D. E. Kinnison, and P. Konopka (2007), On the use of nonmethane hydrocarbons for the determination of age spectra in the lower stratosphere, *J. Geophys. Res.*, *112*, D12208, doi:10.1029/2006JD007686.

1. Introduction

[2] Mean age and age spectrum of an air parcel have proven to be very useful concepts in the study of stratospheric transport [*Hall and Plumb*, 1994; *Waugh and Hall*, 2002]. They allow an efficient characterization of the action of transport, and thus provide a quantitative measure for the intercomparison of the different transport schemes used in models, as well as for the comparison between models and the transport in the real atmosphere.

[3] Mean age and age spectrum are based on the insight that any air parcel consists of a mix of fluid elements, each with its individual trajectory. The age spectrum of a stratospheric air parcel is defined as the frequency distribution of the transit times spent by the various fluid elements between their entry into the stratosphere at the tropical tropopause, the general source region of stratospheric air, and the point where the air parcel is observed. The mean age is given by the first moment of the age spectrum [*Hall and Plumb*, 1994].

[4] Age spectrum and mean age at any resolved location are readily computed for numerical models of the stratosphere. To obtain these quantities for the real stratosphere has proven a bit more laborious. Nevertheless, there are by now numerous empirical determinations of the mean age of air in many parts of the stratosphere. They are based on the measurement of tracers such as CO_2 or SF_6 [*Bischof et al.*, 1980; *Schmidt and Khedim*, 1991; *Nakazawa et al.*, 1995; *Boering et al.*, 1996; *Strunk et al.*, 2000; *Andrews et al.*, 2001a; *Maiss et al.*, 1996; *Harnisch et al.*, 1996; *Volk et al.*, 1997, respectively]. For these tracers, which are chemically inert or nearly inert in the stratosphere and have linearly increasing trends in the troposphere, the delay time after which a particular mixing ratio from the tropical tropopause arrives at a given point in the stratosphere corresponds exactly to the mean age at that point [*Hall and Plumb*, 1994].

[5] Empirical age spectra are more difficult to infer. Correspondingly only few such spectra have been published [*Andrews et al.*, 1999; *Johnson et al.*, 1999; *Andrews et al.*, 2001b]. These studies make use of the fact that transient mixing ratio variations, such as interannual variability, or seasonal cycles are superimposed on the general trends of some of the tracers, such as CO_2 and water vapor. As a consequence, the determination of empirical age spectra demands a more detailed database than the determination of mean age: Namely time series of tracer mixing ratios in the various domains of the stratosphere in addition to a detailed history at the tropical tropopause.

[6] There is a different approach to derive stratospheric age spectra. Rather than on a temporal change in the source of one tracer, it relies on a number of tracers that have a

[1] Institut ICG-2: Troposphäre, Forschungszentrum Jülich, Jülich, Germany.
[2] Department of Chemistry, University of California, Irvine, California, USA.
[3] National Center for Atmospheric Research, Boulder, Colorado, USA.
[4] Institut ICG-1: Stratosphäre, Forschungszentrum Jülich, Jülich, Germany.

0148-0227/07/2006JD007686$09.00

constant source but decay with time at different rates. Like the former, the latter also introduces a transport-dependent spatial variation in the stratospheric mixing ratios. In a recent paper, *Schoeberl et al.* [2005] used this approach in a 3-D chemical transport model together with satellite observations of $CFCl_3$, CF_2Cl_2, CH_4, and N_2O to derive stratospheric age spectra.

[7] Here, we pursue two slightly different and complementary variants of this approach. The first considers the simple case, when the decay rates are constant in time and space, and thus independent of the individual trajectory of a fluid element. Then the stratospheric tracer distributions are directly linked to the age spectrum through a Laplace transformation [*Schoeberl et al.*, 2000], which allows an analytical solution. In addition we use a numerical 1-D model with height-dependent life times to obtain age spectra. Both variants are applied to vertical profiles of NMHCs in the stratosphere. These are derived from the data of the DC-8 aircraft flight 20 of the TRACE P campaign flown on 9 April 2001, that during the latter part of the flight encountered a deep intrusion of stratospheric air. The short lifetimes of the NMHCs, a hundred days or less, limit the application to the lower stratosphere and to the section of the age spectrum at short transit times.

2. Database and Data Reduction

[8] The data presented here are part of a large file which is available electronically (http://www-gte.larc.nasa.gov/trace/TP_dat.htm). Figure 1 summarizes the geographical and meteorological situation during the last part of the flight 20. The horizontal projection of the flight track is shown in Figure 1a, and the vertical flight profile is shown in Figure 1b. The latter also includes the contour line of the 100 ppb O_3 mixing ratio derived from the O_3 lidar measurements aboard the DC 8 [cf. *Browell et al.*, 2003; http://asd-www.larc.nasa.gov/lidar/trp/dial_20.html]. It serves as a surrogate for the tropopause altitude. Clearly the flight penetrated well, by about 6 km, into the stratosphere. The symbols distinguish between the samples taken while the air plane moved into the stratospheric intrusion, and samples taken when exiting the intrusion. The latter part of the flight effectively coincides with the final descent of the aircraft to the Dryden Air Base. For brevity the first part of that flight leg will be called "ascent" and the second part "descent."

[9] Wind speed and direction at the sampling positions are also indicated (Figure 1a). The wind direction veered from west northwest at the beginning of the stratospheric part of the flight track to west south west at its end. The wind speed varied from about 75 km/h at 129°W longitude to about 150 km/h at 122°W longitude, where the maximum penetration into the stratosphere and the maximum wind speeds were reached.

[10] The backward trajectories for the two parts of the flight track are quite different. Three days earlier the air masses sampled during descent were clearly lined up along the western coastline of North America between about 46°N and 58°N latitude, whereas the air masses encountered during ascent were spread over the mid Pacific with a center at about 35°N latitude and 170°W longitude. In addition to different geographic origins of these air masses, their PV values, the so-called RDF-PV (RDF, reverse domain filling), show also systematic differences. In particular, air masses observed during the descent are characterized by high and constant PV values (>4 PVU) while the air sampled during the ascent shows smaller and much more variable RDF-PV values between 2 and 6 PVU Thus we conclude that during the first part of the flight track, the composition of the observed air was influenced by mixing across the tropopause, whereas during the descent much older air masses from the lowermost stratosphere were sampled.

[11] Figure 1 also contains the mixing ratio profiles of the trace gases O_3, CF_2Cl_2 (Figure 1c), and C_2H_6, C_3H_8 (Figure 1d), for better comparison also plotted against longitude. As to be expected for a pair of tracers with stratospheric and tropospheric origin, respectively, the mixing ratio profiles of O_3 and CF_2Cl_2 are strongly anticorrelated. CF_2Cl_2 reaches a minimum mixing ratio of 468 ppt, O_3 a maximum mixing ratio of 697 ppb between 122°W and 121°W longitude; they define the maximum penetration into the stratosphere. C_2H_6 and C_3H_8, two additional tracers of tropospheric origin, show a similar behavior as CF_2Cl_2 except that their mixing ratios decrease much faster with penetration into the stratosphere because of their short lifetimes. In fact, the C_3H_8 mixing ratio drops below 3 ppt, the detection limit of the gas chromatographic NMHC measurement [*Colman et al.*, 2001].

[12] To convert the horizontal plots into vertical profiles, we need an unequivocal height scale. The complicated geometry of the intrusion (Figure 1b) makes it obvious that we cannot directly use the altitude of sample collection as the height coordinate. For the present we choose instead the CF_2Cl_2 mixing ratio as the vertical coordinate. Like N_2O, which is often used for that purpose, it decreases on average monotonically with altitude in the stratosphere. Its advantage here is that CF_2Cl_2 was measured from the same samples as the NMHCs.

[13] Examples of the resulting vertical profiles are shown in Figure 2. Depending on the origin and lifetime of the trace gas considered four different categories of vertical profiles can be distinguished: Gases with a constant tropospheric source, which are nearly inert in the lower stratosphere, but have strong losses at higher altitudes, such as CH_3Cl or CF_2Cl_2, are vertically distributed in the same manner. As a consequence CH_3Cl when plotted against CF_2Cl_2 shows a linear decrease in that height scale. In contrast, a gas of stratospheric origin and virtually inert in the lower stratosphere, such as O_3, exhibits a linear increase with CF_2Cl_2 as the height scale. Gases with an increasing tropospheric source and conserved everywhere in the stratosphere and above, such as CO_2, have a very slight but curved decrease in the lower stratosphere. For these three types of gases the vertical distributions are dominated by mixing. Finally, for gases such as C_2H_6, which have a constant tropospheric source, but have lifetimes that are small compared to the timescale of vertical transport in the lower stratosphere, we observe a strong, apparently exponential decrease against CF_2Cl_2 as the height coordinate. For all four gas types there is reasonably good agreement between the data from ascent and descent: Apart from the tropospheric values the respective data points agree within their scatter and the resulting profiles from both data sets have the same functional forms.

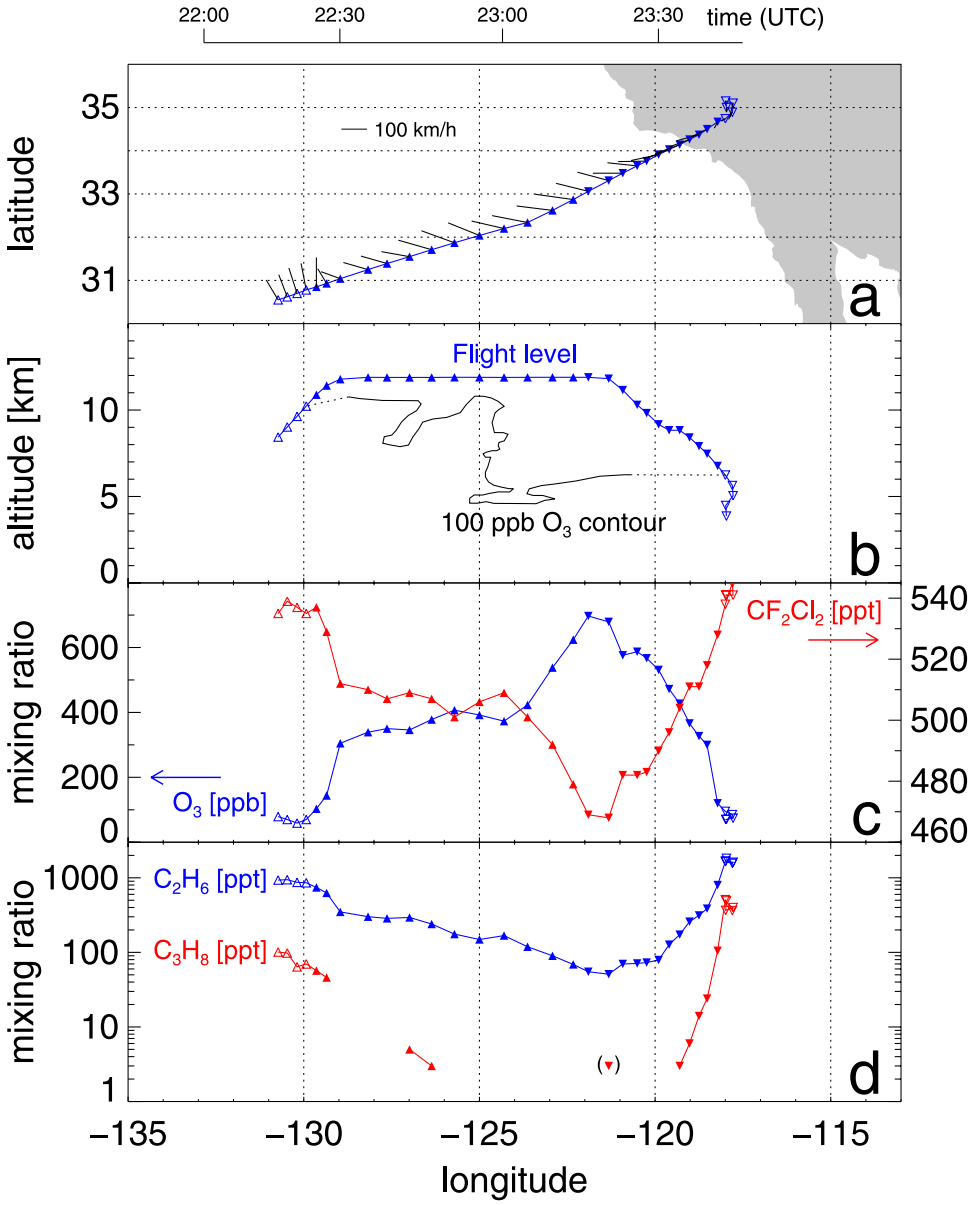

Figure 1. Flight track of the last section of flight 20 of TRACE P flown 9 April 2001 and mixing ratio profiles of O_3, CF_2Cl_2, C_2H_6, C_3H_8 along the flight track. (a) Horizontal projection of the flight track. Triangular symbols indicate the position of sampling, and dashes indicate the wind vector. Upward pointing triangles refer to samples collected while the aircraft moved into the stratospheric intrusion, and downward pointing triangles refer to those when exiting the intrusion. Solid symbols indicate samples collected in the stratosphere, and open symbols indicate those collected in the troposphere. (b) Flight level and the 100 ppb isoline of the O_3 mixing ratio [*Browell et al.*, 2003] serving as indicator of the tropopause. (c) Mixing ratios of O_3 (left-hand scale) and CF_2Cl_2 (right-hand scale) as function of longitude. (d) Mixing ratios of C_2H_6, and C_3H_8 as function of longitude. For further reference a (nonlinear) time axis (UTC) is given at the top.

2.1. Vertical Profiles of Short-Lived Trace Gases

[14] The fact that short-lived gases decrease exponentially with CF_2Cl_2 as the height coordinate is emphasized in Figure 3. It summarizes the vertical profiles of the gases $CHCl_3$, CO, C_2H_6, C_2H_2, C_3H_8, n-C_4H_{10} observed during ascent and descent. All of these gases have short lifetimes, varying between about one week and two years in the lower stratosphere, and all those gases decrease exponentially as demonstrated by this semilogarithmic plot of their mixing ratios versus CF_2Cl_2. This holds in particular for the data collected during descent. A fit of a straight line to the latter data yields the characteristic scale height of the exponential decrease, ζ_f, where the index f indicates CF_2Cl_2 as height scale. The ζ_f are listed in Table 1 along with their errors. For later reference the mean standard deviations of the data points from the fitted exponential decreases were also calculated, and incorporated in Table 1. As to be expected: The shorter the lifetime the faster the decrease (see Table 1).

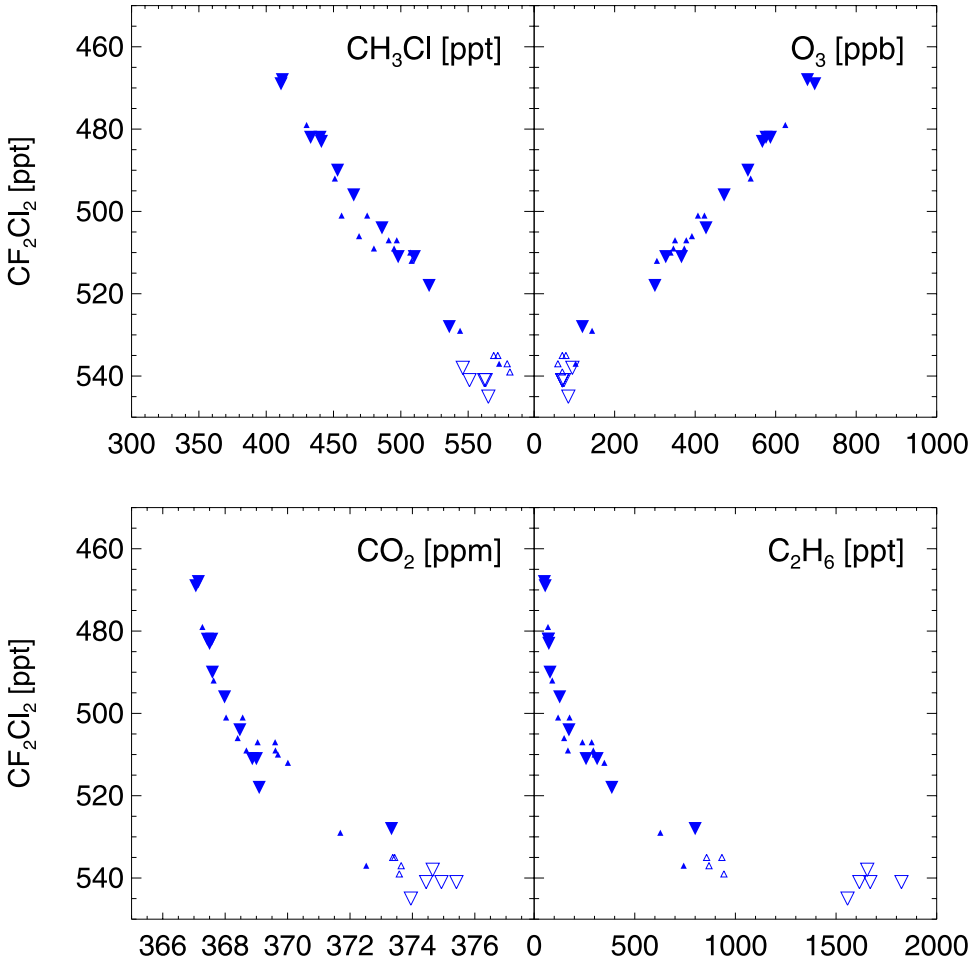

Figure 2. Vertical profiles of CH_3Cl, O_3, CO_2 and C_2H_6 in the lower stratosphere with CF_2Cl_2 as the height scale from flight 20. The definition of the symbols is the same as in Figure 1. Samples collected during descent are represented by larger symbols.

The agreement between ascent and descent is good for the gases CO, C_2H_6, C_3H_8, apart from differences in the mixing ratios in the troposphere, which point to a tropospheric gradient away from the North American continent. It is, however, not so good for the vertical profile of $CHCl_3$ which during ascent deviates strongly from an exponential decay in the altitude range of 510 to 490 ppt CF_2Cl_2. A similar deviation is also found for CH_2Cl_2 (not shown here), and is also expressed in the profile for C_2H_2. Thus it appears real and not an artifact of the measurement. At present there is no good explanation for it.

[15] For reasons given below we do not include $CHCl_3$ in our further analysis. Nevertheless, the scatter in its profile during ascent serves as a warning that an individual vertical profile of a short-lived trace gas in the lower stratosphere may not necessarily follow an exponential decrease, even with CF_2Cl_2 as the vertical scale and even when other, simultaneously measured, short-lived trace gases do show such a behavior.

[16] The trace gas data measured during descent indicate that at least on this occasion the vertical profiles of short-lived tracers in the lower stratosphere are well approximated by an exponential decrease. Such an exponential decrease is also found for the NMHC data from the POLARIS campaigns, 1996 and 1997, albeit with a much larger scatter (F. Flocke, private communication, 2005). Thus an exponential decrease may very well represent the average pattern in the lower stratosphere. This observation is quite useful, because it provides a single parameter description of the vertical distributions of short-lived trace gases and thus a simple way of comparing them.

[17] Obviously the data for n-C_4H_{10} in Figure 3 with only one sample from the stratosphere are not sufficient to derive a reliable value for the characteristic scale height. We therefore attempt another approach and correlate n-C_4H_{10} with C_3H_8 (Figure 4). This leads to a relation with less scatter, though it does not augment the number of stratospheric samples. The characteristic scale height for n-C_4H_{10} given in Table 1 is based on the slope of the correlation in Figure 4 and the characteristic scale height for C_3H_8 from Figure 3.

[18] Finally, the CO values plotted in Figure 3 represent the directly measured mixing ratios. On the other hand stratospheric CO has another source besides the influx from the troposphere, namely the local oxidation of CH_4. In the lower stratosphere, where the reaction of CH_4 is slow, this

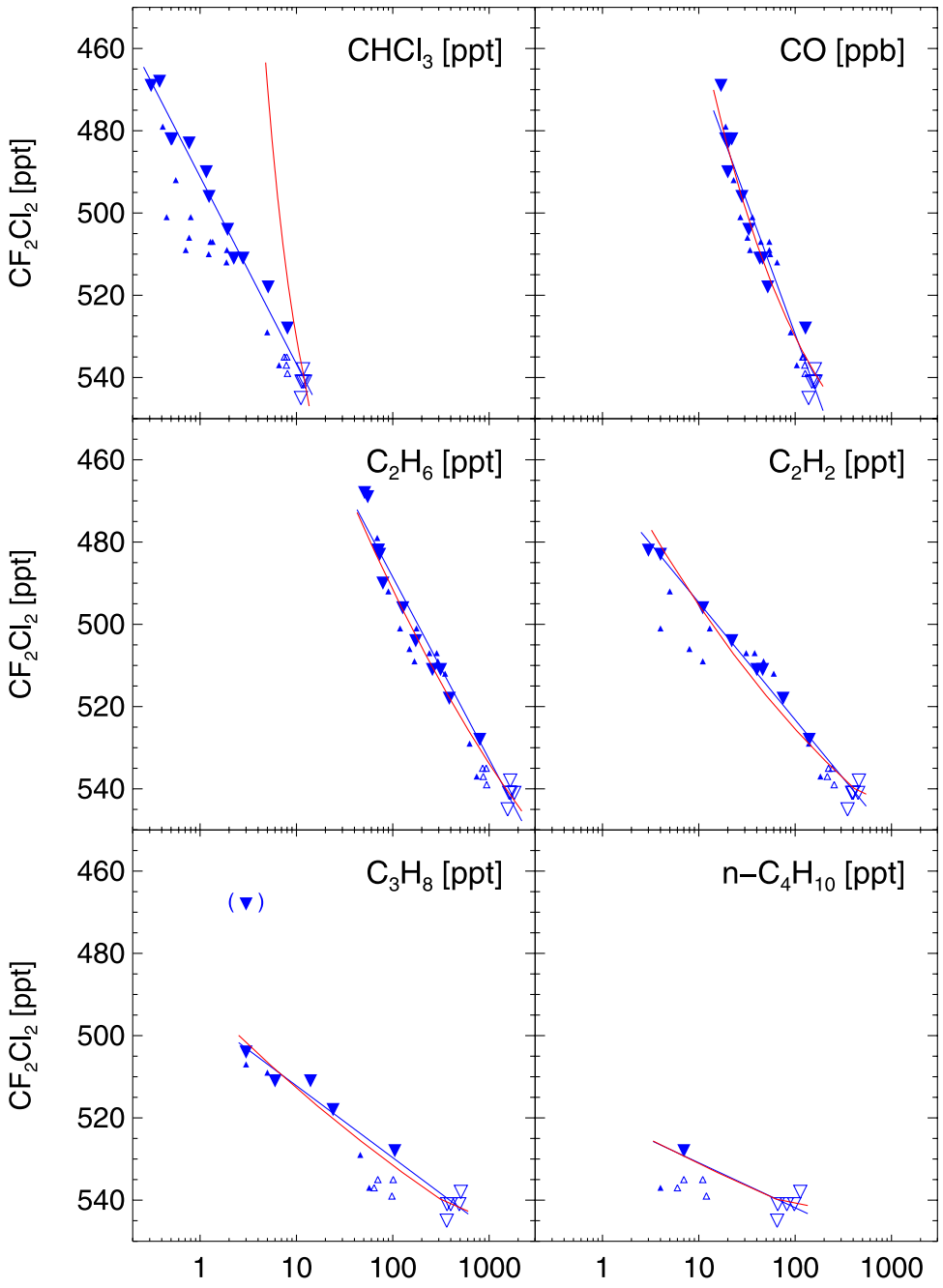

Figure 3. Vertical profiles of $CHCl_3$, CO, C_2H_6, C_2H_2, C_3H_8, and n-C_4H_{10} in the lower stratosphere with CF_2Cl_2 as the height scale from flight 20. The definition of the symbols is the same as in Figure 1. Samples collected during descent are represented by larger symbols. The straight lines represent fits of exponential functions to the data collected during descent. The respective scale heights are given in Table 1. The red curves represent vertical profiles calculated numerically from a 1-D model (see section 3.2).

contributes about 5 ppb of CO, which in principle needs to be corrected for. If we subtract 5 ppb from the directly measured CO mixing ratios we still obtain an exponential decrease but with a scale height of 24.8 ± 1.3 ppt CF_2Cl_2 instead of 27.7 ± 1.6 ppt calculated from the directly measured data and listed in Table 1. Since the difference is relatively small, just barely within the respective 1σ errors, and the correction has an uncertainty of its own, we will proceed using the scale height for the directly measured CO values.

2.2. Relation of the CF_2Cl_2 Height Scale to Geometric Altitude

[19] For better comparison with existing vertical trace gas profiles we would like to relate the CF_2Cl_2 height scale to geometric altitude. This is not possible from the data of

Table 1. Experimental Scale Heights, ζ_f, From Figure 3, Height-Dependent Chemical Lifetimes, $\bar{\tau}_i$ (z) = $\tau_{i,0}$ exp(−z/h), and Average Lifetimes, τ_i, From Equation (1) for the Trace Gases $CHCl_3$, CO, C_2H_6, C_2H_2, C_3H_8, and n-C_4H_{10}[a]

Gas	ζ_f, ppt CF_2Cl_2	k_{OH}, cm^3/s	f_{kOH}	k_{Cl}, cm^3/s	τ,[b] days	$\bar{\tau}$, days	σ_m, ppt CF_2Cl_2	σ_e, ppt CF_2Cl_2
$CHCl_3$	20	$3.1\cdot10^{-14}$		$1.8\cdot10^{-14}$	745	745		
CO	27.7 ± 1.6	$1.7\cdot10^{-13}$	1.3	$3\cdot10^{-14}$	136	136	4.36	5.23
C_2H_6	19.1 ± 0.8	$6.1\cdot10^{-14}$	1.25	$5.1\cdot10^{-11}$	$127\cdot e^{-z/7}$	107	3.81	3.99
C_2H_2	12.4 ± 0.7	$3.8\cdot10^{-13}$	1.4	$4.2\cdot10^{-11}$	$48.1\cdot e^{-z/12.5}$	44.7	3.53	2.38
C_3H_8	7.9 ± 0.6	$4.7\cdot10^{-13}$	1.36	$1.4\cdot10^{-10}$	$28.3\cdot e^{-z/7}$	26	3.04	2.78
n-C_4H_{10}	4.6 ± 0.4	$1.7\cdot10^{-12}$	1.36	$1.4\cdot10^{-10}$	$11.3\cdot e^{-z/7}$	10.7	2.55	2.89

[a]Also given are the rate constant for the reactions with OH and Cl, k_{OH} and k_{Cl}, the error factor of k_{OH}, f_{kOH}, all for the temperature T = 216 K and the pressure 200 hPa [*Sander et al.*, 2003; *Atkinson et al.*, 2002], and the mean standard deviations of the measured data from the fitted exponential decreases, σ_e, and from the numerically calculated profiles, σ_m.
[b]The tropopause values, $\tau_{i,0}$, are based on OH = $5\cdot10^5$ cm^{-3} and Cl = $1.2\cdot10^3$ cm^{-3} (see text). The height, z, is in km.

flight 20 alone; it rather requires an average profile of CF_2Cl_2 in geometric altitude. Measured profiles are scarce for the years bracketing 2001. An earlier average CF_2Cl_2 profile from mid latitudes in Europe covering the period from 1988 to 1991 suggests a linear decrease in the lower stratosphere to about 19 km altitude [*Fabian et al.*, 1996], but is likely to be influenced by the then still significant increase in tropospheric CF_2Cl_2. Two more recent individual profiles from 1996 and 1998 over New Mexico, 34°N, also indicate an approximately linear decrease of CF_2Cl_2 in the lower stratosphere up to 20 km altitude [*Moore et al.*, 2003]. However, for further and more detailed information we have to turn to the CF_2Cl_2 distributions generated by 3-D models. Figure 5 shows the zonally and monthly averaged profiles of CF_2Cl_2 for April and the latitudes 32.9, 35.7, 38.6, 41.4, and 44.3°N. They were generated in a special run of the MOZART-3 model with WACCM 1b meteorological fields and a 106 species chemical mechanism [*Kinnison et al.*, 2007]. Since that run did not cover the year 2001, we chose the profiles from 1999. By that time the tropospheric increase of CF_2Cl_2 had already flattened out, so that they should closely represent the distribution for 2001 as well. All the profiles in Figure 5, even those north of 40°N latitude which are slightly undulating are quite closely approximated by a linear decrease between 10 km and 18 km altitude, with slopes systematically increasing with latitude. Thus we conclude that on average the CF_2Cl_2 height scale correlates linearly with geometric altitude for the stratospheric altitude range considered here. To determine the slope we use the data from the present flight (Figure 1): At the point of deepest penetration into the stratosphere the vertical distance between flight level and tropopause was 12 km − 6 km = 6 km in geometric altitude, and 469 ppt − 538 ppt = −69 ppt in the CF_2Cl_2 height scale. (The value of 538 ppt corresponds to the CF_2Cl_2 mixing ratio observed at 100 ppb of O_3 when the aircraft exited the stratospheric intrusion). From these numbers we deduce a slope of −11.5 ppt/km, i.e., $z_f \sim -11.5$ z. With a precision of 3.5 ppt for the measurement of CF_2Cl_2 and an estimated uncertainty of 0.5 km in the tropopause altitude derived from O_3 this slope has a relative 1σ uncertainty of 11%. As is apparent from Figure 5, slopes that steep begin and extend northward from 44.3°N. This is consistent with our earlier observation that the air masses encountered during descent had recently been advected from the north. Assuming an average tropopause height of 12 km the observed trace gas profiles cover the height range of 12 km to 18 km. The empirical observation that CF_2Cl_2 varies linearly with height over the altitude range considered not only provides a simple justification for the use of CF_2Cl_2 as height coordinate in the presentation of the data, it also allows an analytical determination of the age spectra. Moreover, since the slope of the linear decrease in CF_2Cl_2 is

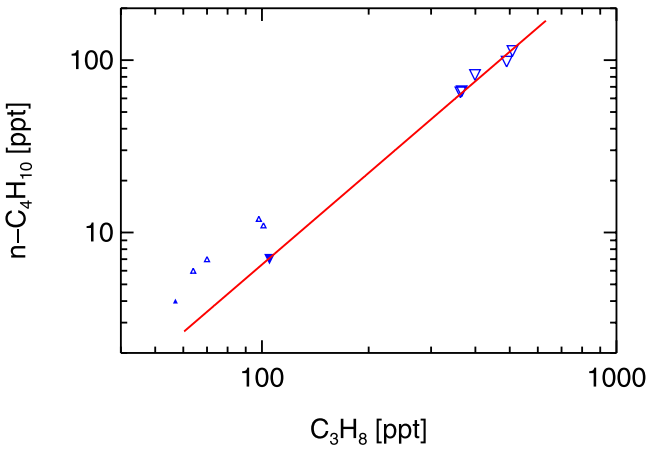

Figure 4. Correlation between the mixing ratios of C_3H_8 and n-C_4H_{10} for the determination of the scale height in the vertical decrease of the n-C_4H_{10}.

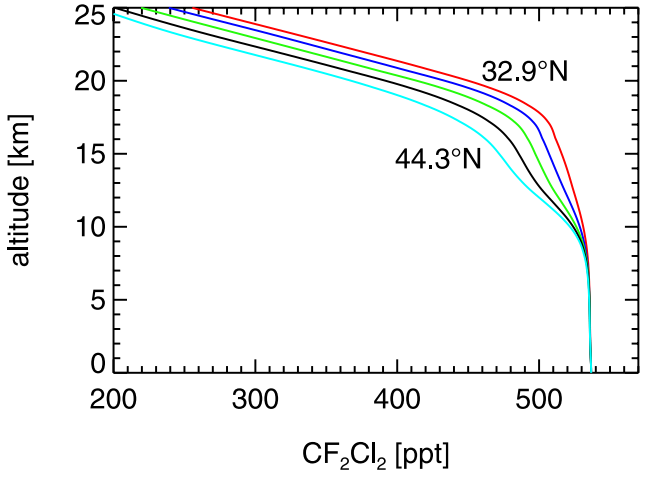

Figure 5. Zonally and monthly averaged vertical profiles of CF_2Cl_2 for April and the latitudes 32.9, 35.7, 38.6, 41.4, and 44.3°N generated by MOZART 3 (see text for details).

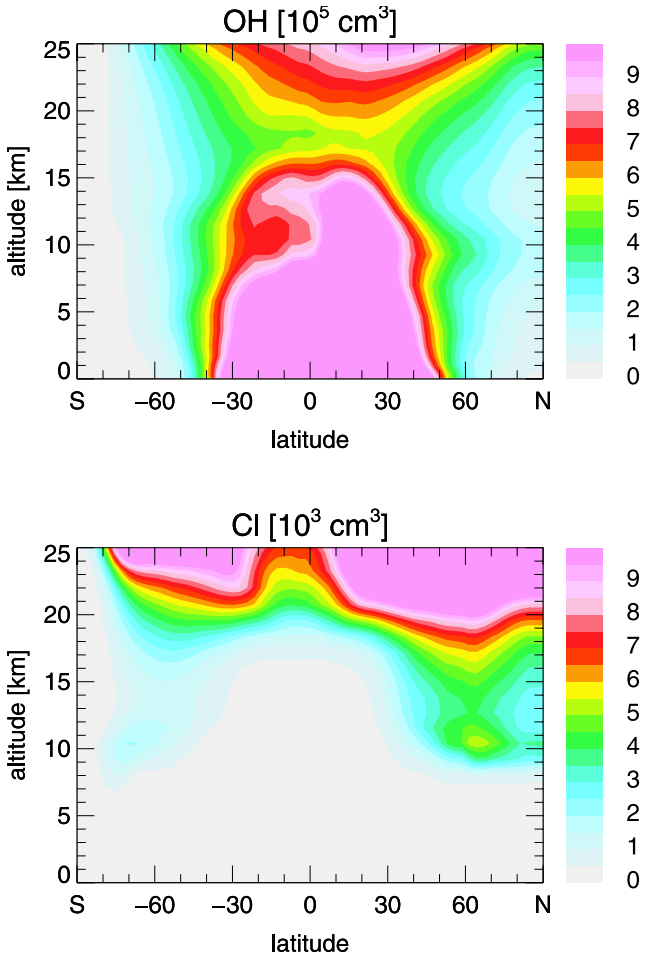

Figure 6. Monthly averaged meridional distributions of the concentration of (top) OH and (bottom) Cl for April generated by MOZART 3 (see text for details).

relatively well constrained, the impact of its uncertainty on the analytical age spectrum can be obtained by a straightforward error propagation (see section 3.1). In the following we will retain CF_2Cl_2 as height coordinate because it is the quantity directly observed from our data.

2.3. Lifetimes of Short-Lived Trace Gases

[20] The trace gases listed in Figure 3 are destroyed in the stratosphere by several mechanisms. Most important are the reactions with OH and Cl. All the other loss processes: Photolysis, reaction with O_3, O^1D, O^3P, and Br are negligible in the height range considered here. The rate constants for the reactions with OH and Cl, k_{OH} and k_{Cl}, at the temperature T = 216 K and the pressure p = 200 hPa are also listed in Table 1.

[21] For the calculation of the lifetimes the concentration fields of OH and Cl, in particular their vertical distributions are also required. The height dependence of OH appears to be small. The measurements by *Hanisco et al.* [2001] showed the OH concentration in the lower stratosphere to depend essentially on the solar radiation and not on the location, i.e., to be independent of altitude. Similar results are found in 3-D model calculations. Figure 6 (top) portrays the mean meridional OH field for April calculated from the same MOZART-3 run as the CF_2Cl_2 profiles. It varies less than 20% in the lower stratosphere at equatorial and northern mid latitudes. We, therefore, assume the OH concentration to be constant with altitude. Since stratospheric air originates at the tropical tropopause it must spend an appreciable part of its transit time south of the latitude of the observation point. This should also be true in the present case, although the immediate trajectories of the air masses originated at around 50°N latitude. We therefore assign a value of 5×10^5 cm^{-3} to the OH concentration, the average value south of 30°N latitude in the lower stratosphere.

[22] In contrast to OH the Cl concentration increases considerably with altitude (Figure 6, bottom): For example, at 30°N from about 1.2×10^3 cm^{-3} at 12 km altitude to 5.6×10^3 cm^{-3} at 20 km altitude (corresponding to 470 ppt CF_2Cl_2 in the model), i.e., more than a factor of 4. As a consequence the alkanes, which react significantly also with Cl, exhibit a marked decrease in lifetime with height. The lifetime of C_2H_6, for instance, which exhibits the largest change, decreases from 127 days at the tropopause to 37 days at 20 km altitude. The lifetimes of the gases, CO, and $CHCl_3$ which react mainly with OH, are virtually constant with altitude. For simplicity the height dependence of the lifetimes is approximated by an exponential function, for the alkanes with a scale height, h, of 7 km representing the common average. For C_2H_2 whose reactivity with Cl is lower, a scale height of 12.5 km is used. The lifetimes at the tropopause (12 km) based on the above OH and Cl concentrations and their exponential decreases with altitude are also listed in Table 1.

[23] To account for the height dependence of the lifetimes and retain the advantage of a single parameter characterization, we also calculate the lifetimes averaged over the trace gas columns in the observed altitude range:

$$\overline{\tau}_i = \frac{\int_{540}^{470} \rho(z_f) \cdot m_i(z_f) \cdot \tau_{i,0} \cdot \exp(-z_f/h_f) dz_f}{\int_{540}^{470} \rho(z_f) \cdot m_i(z_f) dz_f} \quad (1)$$

[24] Here $\rho(z_f) = \rho_0 \cdot exp(-z_f/80)$ is the air density, $m_i(z_f) = m_{i,0} \cdot \exp(-z_f/\zeta_{f,i})$ the mixing ratio, both in the CF_2Cl_2 height scale, and the index 0 refers to the tropopause values. With the slope of the CF_2Cl_2 profile given above the density scale height of 7 km transforms into $H_f = 80$ ppt in the CF_2Cl_2 height scale.

[25] The so averaged $\overline{\tau}_i$ are also listed in Table 1. They do not differ as much from the $\tau_{i,0}$ at the tropopause as one might have expected from the steeply increasing Cl profile: especially the average τ for n-C_4H_{10}, which is quite close to τ_0 at the tropopause, because this gas does not penetrate deeply enough into the stratosphere to experience the higher Cl concentrations.

[26] Given the large uncertainty factors in the rate constants and the uncertainties in the radical concentrations, the lifetimes, $\overline{\tau}_i$ and $\tau_{i,0}$ turn out to be much more uncertain than the scale heights $\zeta_{f,i}$.

2.4. Relation Between $\zeta_{f,i}$ and τ_i

[27] The experimental scale heights $\zeta_{f,i}$ derived in section 2.1 are closely related to the average lifetimes, $\overline{\tau}_i$,

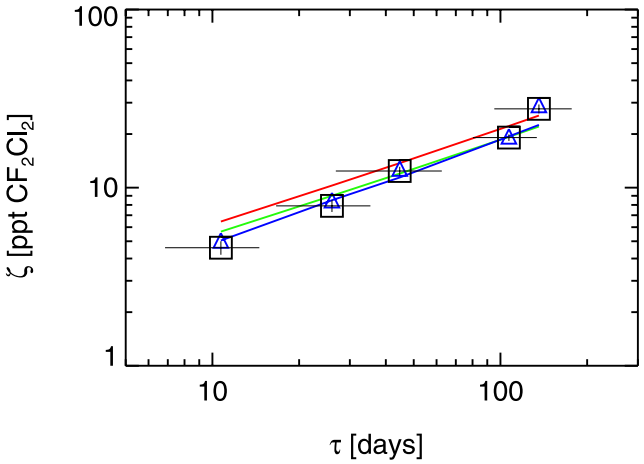

Figure 7. Empirical and modeled relations between scale height ζ_f and the average lifetime $\bar{\tau}$. The empirical data points are indicated by the squares, whose vertical extent exceeds the error in the $\zeta_{f,i}$. The horizontal error bars represent the error contributed by the uncertainty in the reaction rate with OH alone. The green line represents a fit of equation (9) for $\zeta(\tau)$ to all five empirical data points, and the red line represents a fit to the data from CO and C_2H_2 only. The $\zeta_{f,i}$ obtained numerically from a 1-D model and height-dependent lifetimes are indicated by the open triangles. The blue line, $\zeta_{f,m}(z)$, is numerically calculated for tracers with an exponential decrease in τ and a scale height of 7 km.

specified in the preceding section. When plotted against each other (Figure 7) the data points indicate that there is an unequivocal functional relation, $\zeta_f = \zeta_f(\tau)$, between the scale heights and the corresponding average lifetimes in the lower stratosphere. Despite the uncertainties in $\zeta_{f,I}$ and $\bar{\tau}_i$, $\zeta_f(\bar{\tau})$ seems to be fairly tightly characterized at least over the range covered by the present data. The error in the scale heights is contained within the vertical extent of the symbols of Figure 7. The error bars represent the error contributed by the uncertainty of k_{OH} alone, obviously an underestimate of the total error in $\bar{\tau}_i$ It serves, however, to demonstrate that the errors in the $\bar{\tau}_i$ are much larger than those in the $\zeta_{f,i}$.

[28] Plotted in Log/Log format as in Figure 7 the data points appear to follow a straight line. Although we will make no further use of it here, for reference we mention that a fit yields:

$$log\zeta_f = (-0.0406 \pm 0.04) + (0.68 \pm 0.04) * log\ \bar{\tau}, \qquad (2a)$$

$$\text{or } \zeta_f = (0.87 * \bar{\tau})^{0.68}, \qquad (2b)$$

where τ is in units of days, ζ_f in ppt.

[29] We note that $CHCl_3$ is not included in Figure 7: A gas with a lifetime of 745 days, i.e., of more than 2 years, cannot be regarded as short-lived in the lower stratosphere. On the other hand, the ζ_f found empirically for $CHCl_3$ is only 20 ppt, about the same as that for C_2H_6 which has a much shorter lifetime of 107 days. The same applies to CH_2Cl_2 with very nearly the same theoretical lifetime and empirical scale height as $CHCl_3$. This points to an inconsistency. Either there is a significant sink missing from our calculation of the lifetimes of $CHCl_3$ and CH_2Cl_2 or the measurement of these two substances is biased by losses during collection or storage of the air samples. In either case they currently fall outside the ensemble of trace gases considered here, and we will continue to rely on the relation $\zeta_f(\tau)$ as defined by the 5 gases, CO, C_2H_6, C_2H_2, C_3H_8, n-C_4H_{10}.

[30] We also note that with an explicit expression for $\zeta_f(\tau)$ the observed exponential decrease with height of these gases can be stated as a function of τ:

$$m_i(z_f) = m_{i,0} \cdot \exp(-z_f/\zeta_f(\tau_i)) \qquad (3)$$

3. Discussion

[31] To relate the observed vertical trace gas distributions to the age spectrum we use two approaches. First, with a few simplifying assumptions and the 1-D vertical diffusion equation we derive an analytical expression for the exponential decrease. This at the same time gives an analytical expression for the dependence of the scale heights on the lifetimes, and provides some theoretical insight into what controls $\zeta_{f,i} = \zeta_f(\tau_i)$. Second, we solve the 1-D vertical diffusion equation numerically. This allows one to relax the assumptions and still obtain an age spectrum through a fit of the modeled trace gas profiles to the experimental ones by optimizing the profile of the vertical eddy diffusion coefficient, K.

3.1. Simplified Analytical Solution

[32] The first simplification assumes that the lifetimes are constant in time and space. Then the stratospheric steady state distribution of a tracer with a constant mixing ratio $m_{i,0}$ at the (tropical) tropopause and a lifetime τ_i can be directly expressed by the age spectrum [cf. *Schoeberl et al.*, 2000]:

$$m_i(X, \tau_i) = m_{i,0} \cdot \int_0^\infty \exp(-t/\tau_i) \cdot G(X, t)dt \qquad (4)$$

[33] $G(X, t)$ is the age spectrum at the position $X(x, y, z)$. Equation (4) can be understood intuitively. The age spectrum in the integral provides the weighting function with which transport trajectories of different transit times, t, contribute to the mass of the air parcel observed at X. The term $exp(-t/\tau_i)$ describes the fraction of the original mixing ratio at the tropical tropopause left after traveling for the transit time. Since τ_i is constant in space and time, this fraction depends only on the transit time, but not on the actual path taken. The integral over time then represents the local steady state mixing ratio of the tracer generated by adding up the various contributions. Equation (4) also makes it clear that tracers with increasing τ_i probe increasing parts of the age spectrum and that in general it will need a number of such tracers to determine G(X, t).

[34] The integral in equation (4) constitutes a Laplace transform, i.e., $m_i(X, \tau_i)$ normalized by the constant factor

$m_{i,0}^{-1}$ is the Laplace transform of $G(X, t)$. Thus, conversely, if we know the stratospheric trace gas distribution and its dependence on τ_i, we should in principle be able to obtain $G(X, t)$ through an inverse Laplace transform of $m_i(X, \tau_i)$. Equation (4) holds generally. It can be further simplified when we adapt it to the present case, where we only consider the vertical dimension, z, by assuming that transport is facilitated by a 1-D vertical diffusion model with a constant eddy diffusion coefficient, K. In this case the age spectrum is known [*Hall and Plumb*, 1994]:

$$g(z,t) = \frac{z}{\sqrt{\pi \cdot 4 \cdot K \cdot t^3}} \cdot \exp\left(\frac{z}{2H} - \frac{K \cdot t}{4 \cdot H^2} - \frac{z^2}{4 \cdot K \cdot t}\right) \quad (5)$$

[35] Equation (5) is the solution of the partial differential equation for the vertical diffusion of an inert tracer with the mixing ratio $m(z, t)$

$$\rho \cdot \frac{\partial m(z,t)}{\partial t} = \frac{\partial}{\partial z}\rho \cdot K \cdot \frac{\partial m(z,t)}{\partial z} \quad (6)$$

for the boundary condition $m(0, t) = \delta(t)$; that is, the tracer mixing ratio is introduced as a pulse at the tropopause, z = 0 and the time t = 0. The air density $\rho = \rho_0 \cdot \exp(-z/H)$. Inserting g(z, t) for the simplified 1-D case into equation (4) yields:

$$m_i(z,\tau_i) = m_{i,0} \cdot \int_0^\infty \exp(-t/\tau_i) \cdot g(z,t)dt \quad (7)$$

[36] In this case the Laplace transform (7) has an analytical solution [see *Schoeberl et al.*, 2000]. It is given by the exponential function:

$$m_i(z,\tau_i) = m_{i,0} \cdot \exp(-z/\zeta(\tau_i)) \quad (8)$$

with

$$\zeta(\tau_i) = \frac{2H}{\left(\sqrt{1 + \frac{4H^2}{K \cdot \tau}} - 1\right)} \quad (9)$$

The vertical mixing ratio profile $m_i(z,\tau_i)$, equation (8) is of course also the solution of the ordinary differential equation

$$\frac{\partial}{\partial z}\rho \cdot K \cdot \frac{\partial m_i(z,\tau_i)}{\partial z} - \rho \cdot \frac{m_i(z,\tau_i)}{\tau_i} = 0 \quad (10)$$

under the appropriate boundary conditions.

[37] Equation (9) provides the desired analytical approximation of the functional dependence of ζ_i on τ_i. It should thus explain the essential features of $\zeta_i(\tau_i)$ apparent in Figure 7. In addition to τ, the independent variable, $\zeta(\tau)$ from equation (9) depends on two parameters, namely the scale height of the air density, H, and the (constant) eddy diffusion coefficient, K. The first parameter is known: H = 7 km in geometric altitude, or 80 ppt when transformed into the CF_2Cl_2 height scale using the mean vertical gradient in CF_2Cl_2 given in section 2.2. By optimizing K we can fit equation (9) to the observational data pairs $\zeta_{f,i}$, τ_i in Figure 7. With a fit to all 5 trace gases we obtain an average $K_{f,5}$ = 2.8 ppt^2/day in the CF_2Cl_2 height scale. The resulting curve $\zeta_{f,5}(\tau)$ is included in Figure 7. Although hard to discern over the short data interval presented in Figure 7, it bends slightly upward for larger τ. We note also, that ζ_f and the fitted K_f depend only weakly on H_f. This is due to the fact that $\tau_i << 4\ H_f^2/K_f$ = 9100 days for all τ_i considered. Indeed for $\tau_i \sim 1$ day ζ_f approaches $(K_f\ \tau)^{0.5}$ and thus becomes independent of H_f which allows a simple geometric solution for K_f by extrapolating $\zeta_{f,5}(\tau)$ to τ_i = 1 day in Figure 7. This also means that the error of 11% in the slope of the CF_2Cl_2 profile introduces only a small error, 2%, in the derived K_f.

[38] When we restrict the set of experimental ζ_i, τ_i to the ones for CO, and C_2H_2, for which the condition of $\tau_i(z)$ = constant is best met, the fit of equation (9) to the data yields a significantly larger average $K_{f,2}$ of 3.6 ppt^2/day. The resulting $\zeta_{f,2}(\tau)$ runs parallel and above $\zeta_{f,5}(\tau)$ (see Figure 7). Both curves agree quite well with the experimental ζ to which they were fitted. This means that the vertical profiles calculated from equation (8) with the above parameters H_f and K_f will match the measured height profiles of the trace gases in Figure 3 reasonably well. Moreover, when $K_{f,2}$ and $K_{f,5}$ are transformed to geometric altitude, z, using the slope of the average CF_2Cl_2 profile given in section 2.2, we obtain K_2 = 0.32 m^2/s and K_5 = 0.25 m^2/s. Both values agree quite well with previous estimates of K in the lower stratosphere [cf. *Ehhalt et al.*, 2004]. In this case, however, the error of 11% in the slope of the CF_2Cl_2 decrease propagates into a large error of 21%. This is due to the fact that the slope enters squared in the conversion of K_f to K.

[39] The derived average K together with the fixed H fully specifies the age spectrum given by equation (5) in geometric or CF_2Cl_2 altitude scales. That means that the so calculated average age spectra have the form suggested by *Hall and Plumb* [1994]. They will be further discussed in section 3.3 below.

3.2. Numerical Calculation of Trace Gas Profiles and $\zeta_{f,i}$ From a 1-D Model

[40] Finally, we employ a simple 1-D model, to numerically calculate the vertical profiles of the 5 trace gases. It also calculates the vertical profile of CF_2Cl_2 with the aim to derive $\zeta_{f,i}$ from the model, and to match them to the experimental values by optimizing the K profile. This implies that the model generated trace gas profiles in the CF_2Cl_2 height scale are kept as nearly exponential as possible. A numerical approach has the advantage that it does not require the approximations of constant τ_i and of constant K. Neither does it require the CF_2Cl_2 profile to be linear with altitude in the lower stratosphere, and indeed the modeled CF_2Cl_2 profile is slightly curved. As a first approach to height-dependent lifetimes we select the $\tau_i(z)$ derived in section 2.3 and listed in Table 1. The loss of CF_2Cl_2 is dominated by the photolysis rate, whose vertical profile is chosen to represent equinox at 30°N latitude.

[41] As it turns out with this selection of $\tau_i(z)$ a surprisingly good fit for all 5 tracers is obtained when a vertical profile of K_m = 0.46 m^2/s, constant with altitude, is used. This agreement is first demonstrated in Figure 3, where the numerically calculated trace gas profiles are superimposed on the measured data. The modeled profiles are not exactly

exponential with CF_2Cl_2 as height coordinate. However, the quality of the fit of the modeled profiles to the data is at least as good as that of the linear regression lines fitted directly to the data. This is underlined by the mean standard deviations of the data from the numerically calculated profiles which are given in Table 1 and compare favorably with those for the linear regression lines. Moreover, the modeled profiles can be well approximated by an exponential decrease. Thus the numerically calculated profiles can also be reduced to a one parameter description. The slight curvature in their semilog plots versus CF_2Cl_2 means, however, that the exponential decrease fitted to the numerically calculated profiles, and thus the model derived $\zeta_{f,i}$ depend slightly on the height interval of the fit. To be comparable with the measurements, we chose the intervals to agree with the respective height ranges over which the data were obtained. In Figure 7 the so calculated $\zeta_{f,i}$ are compared to the experimental ones. The agreement is excellent.

[42] Altogether the numerically calculated trace gas profiles very closely match the measured ones over the full altitude range observed. Nevertheless the result of a constant K profile is not exactly unique: Slightly curved variants of that K profile give similarly good fits. The constant K is adopted as the simplest form of the K profile compatible with the data. We emphasize, however, that now the condition of a constant K is not an a priori assumption, but rather the result of a fit. The apparent difference between the numerically derived K and the analytically calculated ones is exaggerated by two factors: First the average vertical gradient of the modeled CF_2Cl_2 profile is weaker by about 10% than the empirical one adopted in section 2.2 and used in the analytical calculation of K. In the conversion of K_F in the CF_2Cl_2 height scale to K in the geometric height scale that gradient enters squared. This causes a factor of 1.25 difference. The second factor results from the averaging procedure for $\tau(z)$ by equation (1). That weighted average favors the lower altitudes, and results in larger $\overline{\tau}_i$ than would be obtained from an unweighted average. Since $\zeta \sim \mathrm{sqrt}(K*\tau)$ (see section 3.1) this induces a bias toward smaller values in the K derived analytically for a given ζ. The difference in averaging amounts a factor of 1.05 for K_2 and a factor of 1.1 for K_5. Accounting for these two factors leaves an actual ratio of 1.1 between K_2 and K_m and a ratio of 1.34 between K_5 and K_m owing to the introduction of an explicit height dependence in τ.

[43] For further comparison Figure 7 also includes a curve $\zeta_{f,m}(\tau)$, blue line, numerically calculated for tracers with an exponential decrease in τ with a scale height of 7 km (Table 1), and $K_m = 0.46\ m^2/s$. Its gradient is slightly steeper than the analytically derived curves.

[44] Because of the constant K profile the age spectrum derived from the numerical model also has the form of equation (5). In the following section 3.3 it will be compared to the analytical age spectra.

3.3. Age Spectra

[45] Figure 8 compares the model derived age spectrum $g_m(z, t)$, with the two analytical age spectra, $g_5(z, t)$, $g_2(z, t)$, for the altitudes 14 km, 16 km, 18 km and 20 km. These altitudes correspond to CF_2Cl_2 mixing ratios of 545, 530, 512, 487, and 454 ppt, respectively, in the numerical 1-D model calculation. $g_m(z, t)$ can also be obtained numerically from the 1-D model by introducing a δ function shaped pulse of the mixing ratio at the tropopause and following its propagation in time at the various altitudes. The so calculated spectra agree exactly with those derived from equation (5) for the same altitudes.

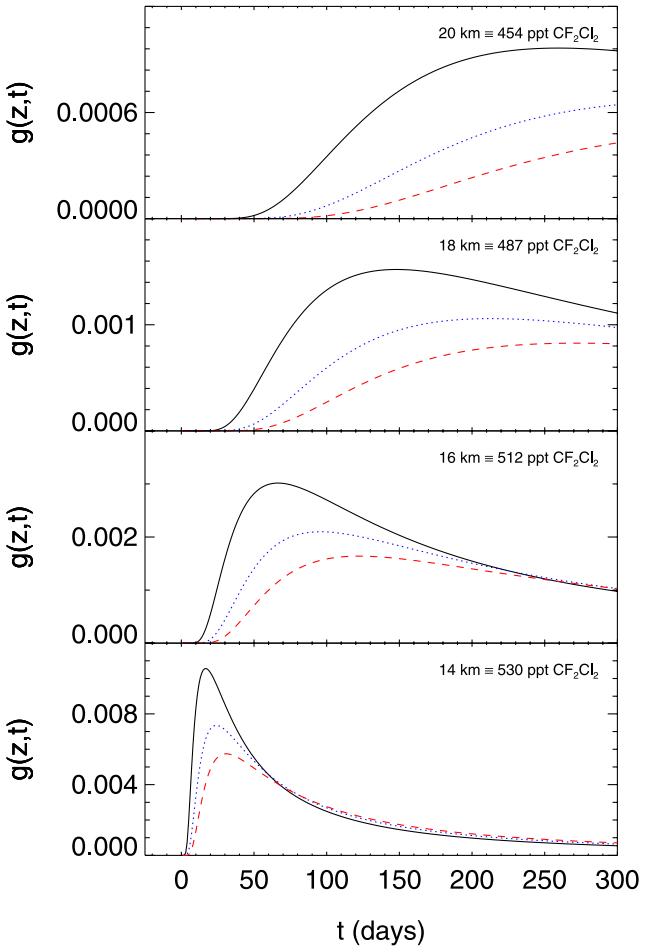

Figure 8. Age spectra for 14 km,16, km, 28 km, and 20 km altitudes derived from the various model fits to the empirical data. They all have the functional form given by equation (5). The solid line represents the numerical fit by the 1-D model and height-dependent τ ($g_m(z, t)$ with $K_m = 0.46\ m^2/s$). The dotted line represents the analytical fit to the data for CO and C_2H_2 ($g_2(z, t)$ with $K_2 = 0.32\ m^2/s$). The dashed line indicates the analytical fit for all five data points ($g_5(z, t)$ with $K_5 = 0.25\ m^2/s$).

[46] The age spectra in Figure 8 are cut off at 300 days. Because of the short lifetimes of the trace gases considered here the age spectrum at longer transit times does not contribute to the integral in equation (7), and thus leaves no signature in the vertical profiles of the mixing ratios. In turn the measured trace gas profiles contain no information about that part of the age spectrum. Consequently this analysis does not allow any statement about the older part of the age spectrum. We note, however, that the age spectra of the form of equation (5) could be extended arbitrarily in time. This corresponds to the implicit assumption that the functional form of ζ, equation (9), would also be applicable at longer lifetimes.

[47] Clearly the three age spectra differ significantly. Because it requires fewer approximations and affords the best fit to all 5 measured trace gas profiles, we consider $g_m(z, t)$ the most realistic of the presented age spectra. Age spectrum $g_2(z, t)$ derived from the 2 trace gases which approximate the condition of constant τ_i is about 30% lower in maximum amplitude and, as expected from its smaller K, expanded in time. The difference provides an indication of the sensitivity of the derived age spectra to the assumptions, mainly about the gradient in the vertical CF_2Cl_2 profile but also about the height dependence of τ_i and its averaging. There are other sources of uncertainty. Probably the most important are the errors in the absolute values of the τ_i. These are given by the errors of the rate constants and by the uncertainties in the OH and Cl fields experienced by the trace gases. Some of these uncertainties, e.g., that in the OH field, may result in a common scaling of the τ_i. An error of this type will translate into a linear contraction or expansion in the timescale of the age spectrum, as suggested by the inverse Laplace transform. Most errors, however, will result in displacements of the τ_i relative to each other. Such displacement could change the form of the $\zeta(\tau)$ curve in Figure 7, and consequently the value of the fit parameter K. It may even require a height-dependent K(z) for optimum fit. A further source of error is the 1-D modeled profile of CF_2Cl_2, and finally the implicit assumption of a stratospheric transport constant in time made here.

[48] All these sources of uncertainty are hard to treat quantitatively within the frame of a simplified 1-D model. The present analysis serves, however, to demonstrate that the distributions of short-lived trace gases contain information about the age spectrum in the lower stratosphere providing good time resolution for the low end of the spectra. Moreover, it allows one to extract information on the most important factor influencing the age spectrum, namely vertical transport. A more detailed, less approximative analysis will require the use of a 3-D model.

[49] In any case, the age spectra derived here are specific for the location and time of the sampling and cannot claim to represent regional or global averages. Although there are a number of age spectra from 3-D chemical transport models in the literature [see *Hall et al.*, 1999; *Waugh and Hall*, 2002], and even a few empirical ones derived from measurements of CO_2 [cf. *Andrews et al.*, 2001a], or other trace gases [*Schoeberl et al.*, 2005], we could find none which would match the latitude and the altitude range considered here. Thus a comparison with published age spectra does not seem feasible.

[50] We can, however, tentatively compare the age of air predicted from the present age spectra, for instance from $g_m(z, t)$, with the mean age profiles in the literature. This obviously implies the assumption that $g_m(z, t)$ can be extrapolated to transit times much longer than those covered by the measured trace gas profiles (see also the beginning of this section). Since $g_m(z, t)$ is of the form given by equation (5) the vertical age profile of stratospheric air, $\Gamma(z)$, is given by

$$\Gamma(z) = \frac{z \cdot H}{K} \tag{11}$$

[51] [*Hall and Plumb*, 1994], where the parameters K = 0.46 m^2/s and H = 7 km are those from $g_m(z, t)$, and z is counted from the tropopause. With these values Γ at 6 km, about the highest altitude above the tropopause reached here, becomes 2, 9 y. This value is in good agreement with the corresponding literature values of Γ(6 km) for 30–35°N latitude [see *Andrews et al.*, 2001b; *Hall et al.*, 1999], which could imply that $g_m(z, t)$ is not too far from the zonal and annual average.

4. Summary and Conclusions

[52] From trace gas measurements during the penetration of a stratospheric intrusion we derived vertical profiles of NMHC and other short-lived trace gases in the lower stratosphere. All these profiles show an exponential decrease with the mixing ratio of CF_2Cl_2 which serves as the altitude scale. This allows describing their vertical distribution by one parameter, the scale height. The empirical scale heights are shown to be related to the respective lifetimes of the trace gases in a unique fashion, $\zeta_i(\tau_i)$. Using the approximation of a 1-D diffusive model with a constant eddy diffusion constant, K, and assuming constant lifetimes we can establish an analytical solution for this relation. By fitting the theoretical expression for $\zeta(\tau)$ to the empirical data we can estimate K and thus obtain an approximate age spectrum. A much better fit to the empirical ζ_i is obtained, when we allow the lifetimes to be height-dependent and calculate the theoretical ζ numerically from a 1-D model. This fit also suggests a constant K_m = 0.46 m^2/s, larger than that obtained from the fit of the analytical solution. The obtained age spectra should be valid for transit times to about 300 days. Because of the short lifetimes, trajectories with longer transit times do not contribute to the observed mixing ratios and thus leave no signature in the vertical trace gas profiles. A simple analysis like the present one can only account for the expression of the most salient factors influencing the derived age spectrum, namely (temporally constant) vertical transport and height-dependent lifetimes. It appears, however, that these are also the dominant factors. The study of other influence factors, such as 3-D transport and lifetimes varying with time, will require the use of an appropriate 3-D model.

References

Andrews, A. E., K. A. Boering, B. C. Daube, S. C. Wofsy, E. J. Hintsa, E. M. Weinstock, and T. P. Bui (1999), Empirical age spectra for the lower tropical stratosphere from in situ observations of CO_2: Implications for stratospheric transport, *J. Geophys. Res.*, *104*(D21), 26,581–26,595.

Andrews, A. E., et al. (2001a), Mean ages of stratospheric air derived from in situ observations of CO_2, CH_4, and N_2O, *J. Geophys. Res.*, *106*(D23), 32,295–32,314.

Andrews, A. E., K. A. Boering, S. C. Wofsy, B. C. Daube, D. B. Jones, S. Alex, M. Loewenstein, J. R. Podolske, and S. E. Strahan (2001b), Empirical age spectra for the midlatitude lower stratosphere from in situ observations of CO_2: Quantitative evidence for a subtropical "barrier" to horizontal transport, *J. Geophys. Res.*, *106*(D10), 10,257–10,274.

Atkinson, R., D. L. Baulch, R. A. Cox, J. N. Crowley, R. F. Hampson Jr., J. A. Kerr, M. J. Rossi, and J. Troe (2002), Summary of evaluated kinetic and photochemical data for atmospheric chemistry, IUPAC Subcomm. on Gas Kinet. Data Eval. for Atmos. Chem., Int. Union of Pure and Appl. Chem., Basel, Switzerland.

Bischof, W., P. Fabian, and R. Borchers (1980), Decrease in CO_2 mixing-ratio observed in the stratosphere, *Nature*, *288*(5789), 347–348.

Boering, K. A., S. C. Wofsy, B. C. Daube, H. R. Schneider, M. Loewenstein, and J. R. Podolske (1996), Stratospheric mean ages and transport rates

from observations of carbon dioxide and nitrous oxide, *Science*, *274*(5291), 1340–1343.

Browell, E. V., et al. (2003), Large-scale ozone and aerosol distributions, air mass characteristics, and ozone fluxes over the western Pacific Ocean in late winter/early spring, *J. Geophys. Res.*, *108*(D20), 8805, doi:10.1029/2002JD003290.

Colman, J. J., A. L. Swanson, S. Meinardi, B. C. Sive, D. R. Blake, and F. S. Rowland (2001), Description of the analysis of a wide range of volatile organic compounds in whole air samples collected during PEM-Tropics A and B, *Anal. Chem.*, *73*, 3723–3731.

Ehhalt, D. H., F. Rohrer, S. Schauffler, and M. Prather (2004), On the decay of stratospheric pollutants: Diagnosing the longest-lived eigenmode, *J. Geophys. Res.*, *109*, D08102, doi:10.1029/2003JD004029.

Fabian, P., R. Borchers, and U. Schmidt (1996), Proposed reference models for CO_2 and halogenated hydrocarbons, in *Cospar International Reference Atmosphere* (*Cira*), part iii, *Adv. Space Res.*, *18*, 145–153.

Hall, T. M., and R. A. Plumb (1994), Age as a diagnostic of stratospheric transport, *J. Geophys. Res.*, *99*(D1), 1059–1070.

Hall, T. M., D. W. Waugh, K. A. Boering, and R. A. Plumb (1999), Evaluation of transport in stratospheric models, *J. Geophys. Res.*, *104*(D15), 18,815–18,839.

Hanisco, T. F., et al. (2001), Sources, sinks, and the distribution of OH in the lower stratosphere, *J. Phys. Chem. A*, *105*(9), 1543–1553.

Harnisch, J., R. Borchers, P. Fabian, and M. Maiss (1996), Tropospheric trends for CF_4 and C_2F_6 since 1982 derived from SF_6 dated stratospheric air, *Geophys. Res. Lett.*, *23*(10), 1099–1102.

Johnson, D. G., K. W. Jucks, W. A. Traub, K. V. Chance, G. C. Toon, J. M. Russell, and M. P. McCormick (1999), Stratospheric age spectra derived from observations of water vapor and methane, *J. Geophys. Res.*, *104*(D17), 21,595–21,602.

Kinnison, D. E., et al. (2007), Sensitivity of chemical tracers to meteorological parameters in the MOZART-3 chemical transport model, *J. Geophys. Res.*, doi:10.1029/2006JD007879, in press.

Maiss, M., L. P. Steele, R. J. Francey, P. J. Fraser, R. L. Langenfelds, N. B. A. Trivett, and I. Levin (1996), Sulfur hexafluoride—A powerful new atmospheric tracer, *Atmos. Environ.*, *30*(10–11), 1621–1629.

Moore, F. L., et al. (2003), Balloonborne in situ gas chromatograph for measurements in the troposphere and stratosphere, *J. Geophys. Res.*, *108*(D5), 8330, doi:10.1029/2001JD000891.

Nakazawa, T., T. Machida, S. Sugawara, S. Murayama, S. Morimoto, and G. Hashida (1995), Measurements of the stratospheric carbon-dioxide concentration over Japan using a balloon-borne cryogenic sampler, *Geophys. Res. Lett.*, *22*(10), 1229–1232.

Sander, S. P., et al. (2003), Chemical kinetics and photochemical data for use in stratospheric modeling, *JPL Publ. 02-25*, Jet Propul. Lab., Pasadena, Calif.

Schmidt, U., and A. Khedim (1991), In situ measurements of carbon-dioxide in the winter Arctic vortex and at midlatitudes: An indicator of the age of stratopheric air, *Geophys. Res. Lett.*, *18*(4), 763–766.

Schoeberl, M. R., L. C. Sparling, C. H. Jackman, and E. L. Fleming (2000), A Lagrangian view of stratospheric trace gas distributions, *J. Geophys. Res.*, *105*(D1), 1537–1552.

Schoeberl, M. R., A. R. Douglass, B. Polansky, C. Boone, K. A. Walker, and P. Bernath (2005), Estimation of stratospheric age spectrum from chemical tracers, *J. Geophys. Res.*, *110*, D21303, doi:10.1029/2005JD006125.

Strunk, M., A. Engel, U. Schmidt, C. M. Volk, T. Wetter, I. Levin, and H. Glatzel-Mattheier (2000), CO_2 and SF_6 as stratospheric age tracers: Consistency and the effect of mesospheric SF_6-loss, *Geophys. Res. Lett.*, *27*(3), 341–344.

Volk, C. M., J. W. Elkins, D. W. Fahey, G. S. Dutton, J. M. Gilligan, M. Loewenstein, J. R. Podolske, K. R. Chan, and M. R. Gunson (1997), Evaluation of source gas lifetimes from stratospheric observations, *J. .Geophys. Res.*, *102*(D21), 25,543–25,564.

Waugh, D., and T. Hall (2002), Age of stratospheric air: Theory, observations, and models, *Rev. Geophys.*, *40*(4), 1010, doi:10.1029/2000RG000101.

D. R. Blake, Department of Chemistry, University of California, Irvine, CA 92697, USA.

D. H. Ehhalt and F. Rohrer, Institut ICG-2: Troposphäre, Forschungszentrum Jülich, D-52425 Jülich, Germany. (f.rohrer@fz-juelich.de)

D. E. Kinnison, National Center for Atmospheric Research, POB 3000, Boulder, CO 80307, USA.

P. Konopka, Institut ICG-1: Stratosphäre, Forschungszentrum Jülich, D-52425 Jülich, Germany.